ACS Chemical Neuroscience

pubs.acs.org/chemneuro Research Article

Phospholipids and Cholesterol Determine Molecular Mechanisms of Cytotoxicity of α-Synuclein Oligomers and Fibrils

Kiryl Zhaliazka, Abid Ali, and Dmitry Kurouski*

Cite This: https://doi.org/10.1021/acschemneuro.3c00671 Read Online

ACCESS | Metrics & More | Article Recommendations | Supporting Information

ABSTRACT: Progressive loss of dopaminergic (DA) neurons in the substantia nigra pars compacta, hypothalamus, and thalamus is a hallmark of Parkinson's disease. Neuronal death is linked to the abrupt aggregation of α-synuclein (α-Syn), a small membrane protein that regulates cell vesicle trafficking. α-Syn aggregation rate, as well as the secondary structure and toxicity of α-Syn fibrils, could be uniquely altered by lipids. However, molecular mechanisms that determine such a remarkable difference in the toxicity of α-Syn fibrils formed in the presence of lipids remain unclear. In this study, we used a set of molecular assays to determine the molecular mechanism by which α-Syn fibrils formed in the presence of phosphatidylcholine (PC), cardiolipin (CL), and cholesterol (Cho) exert cell toxicity. We found that rat dopaminergic cells exposed to α-Syn fibrils formed in the presence of different lipids exert drastically different magnitudes and dynamics of unfolded protein response (UPR) in the endoplasmic reticulum (ER) and mitochondria (MT). Specifically, α-Syn:CL were found to cause the strongest, whereas α-Syn fibrils formed in the absence of lipids had the lowest magnitude of the UPR cell response. We also found the opposite dynamics of the ER- and MT-UPR responses in rat dopaminergic cells exposed to protein aggregates. These results could suggest that facing severe ER stress, dopaminergic cells suppress MT-UPR response, enabling the maximal ATP production to restore their normal physiological function. These findings help to better understand complex mechanisms of cell toxicity of amyloid aggregates and ultimately find neuroprotective drug candidates that will be able to suppress the spread of Parkinson's disease.

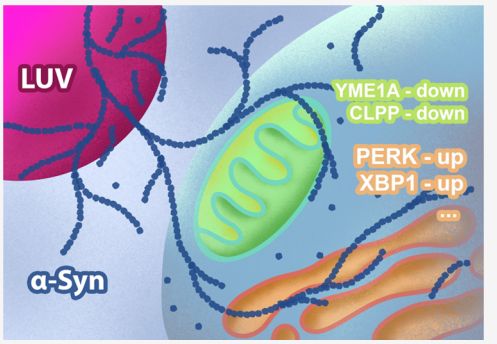

KEYWORDS: *α-synuclein, unfolded protein response, mitochondria, phosphatidylcholine, cardiolipin, cholesterol*

INTRODUCTION

A progressive loss of dopaminergic (DA) neurons in substantia nigra pars compacta (SNc), hypothalamus and thalamus is the hallmark of Parkinson's disease (PD).[1−3] This severe progressive pathology is projected to strike 12 million people by 2040 worldwide.[4] Current treatment methods are not neuroprotective and are largely focused on mitigating the motor dysfunction associated with PD.[5,6] To a large extent, because the underlying molecular causes of PD remain unclear.[5,6]

A growing body of evidence indicates that a loss of DA neurons is linked to an abrupt aggregation of α-synuclein (α-Syn), a small membrane protein that regulates cell vesicle trafficking.[7] Protein aggregation results in the formation of α-Syn oligomers and fibrils, cytotoxic species that can pass from cell to cell causing neuronal death in the caudo-rostral direction.[8−14] Galvagnion and co-workers found that phospholipids could alter the rate of α-Syn aggregation.[15−17] It was also shown that the effect is largely dependent on the lipid-to-protein ratio. Specifically, at the low concentration of lipid bilayers relative to the concentration of the protein, lipid vesicles facilitate protein−protein interactions, which, in turn, trigger α-Syn aggregation.[15−17] However, with an increase in the concentration of lipids relative to the concentration of protein, a decrease in the rate of α-Syn aggregation is observed. These findings suggest that an increase in the overall surface of lipid bilayers lowers the probability of such protein−protein interactions.[15−17] Our group discovered that lipids not only altered the rate of α-Syn aggregation but also modified the secondary structure of α-Syn oligomers formed at the early, middle, and late stages of protein aggregation.[18,19] Furthermore, Dou and co-workers found that phosphatidylcholine (PC) and phosphatidylserine (PS) drastically changed the toxicity of α-Syn oligomers and fibrils formed in their presence.

Recently reported results by Zhaliazka and co-workers showed that such lipid-determined toxicity of oligomers and fibrils could be a general phenomenon typical for a large group of amyloidogenic proteins.[20,21] Specifically, the researchers showed that the secondary structure and toxicity of amyloid

Received: October 17, 2023
Revised: December 20, 2023
Accepted: December 21, 2023

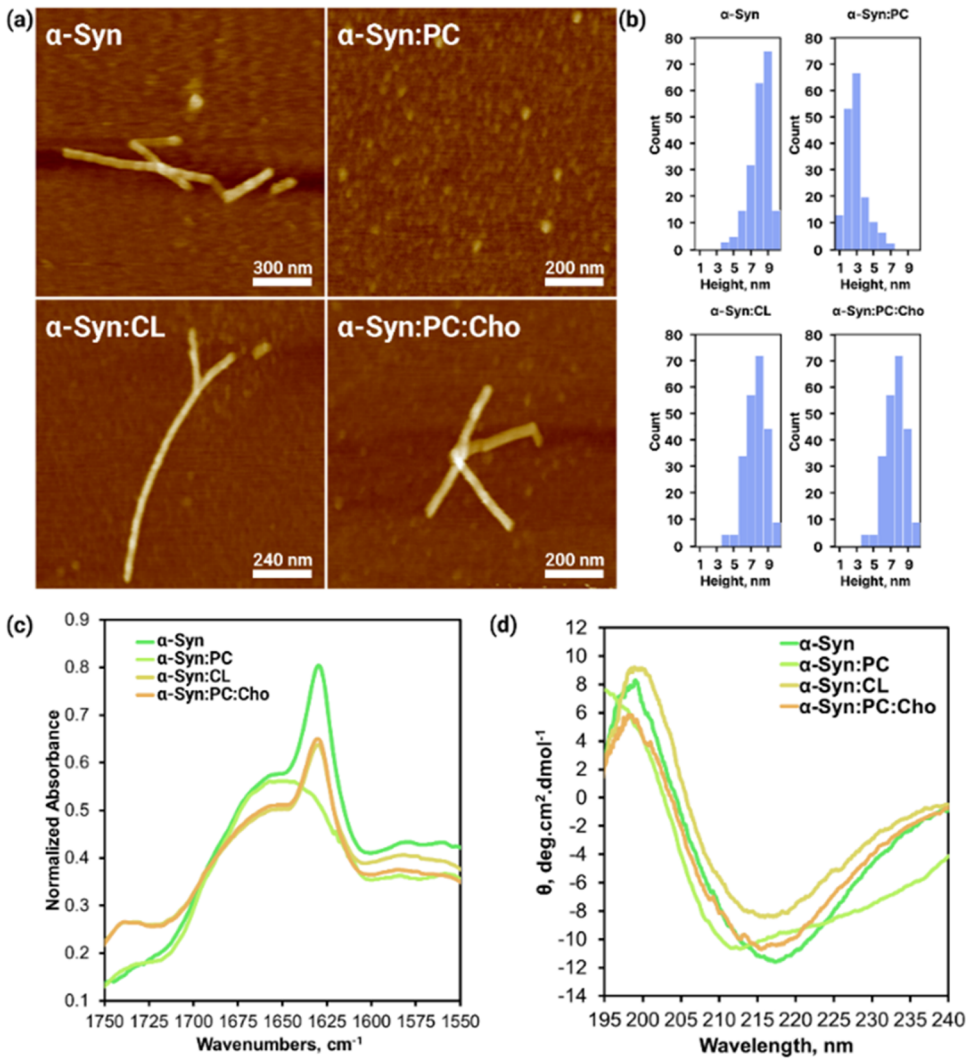

Figure 1. (a) AFM height images of a-Syn fibrils formed after 96 h of protein aggregation, shown for samples grown without and with PC, CL, and PC:Cho LUVs. (b) Height profile corresponding to the AFM images of the a-Syn fibrils. (c) FTIR spectra of a-Syn samples grown without and with PC, CL, and PC:Cho LUVs. (d) CD spectra of a-Syn samples grown without and with PC, CL, and PC:Cho LUVs.

β_{1-42} ($A\beta_{1-42}$) oligomers and fibrils could be uniquely altered by cholesterol (Cho), cardiolipin (CL), and PC.[20] Similar results were also reported by Matveyenka and co-workers for insulin and lysozyme.[22−24]

However, the underlying molecular mechanisms of the differences discussed above in the toxicity that amyloid oligomers and fibrils exert on neurons remain unclear. Matveyenka and co-workers found that amyloid aggregates were endocytosed by cells, which resulted in the irreversible damage of cell endosomes.[23] This caused leakage of protein aggregates into the cytosol, where they damaged endoplasmic reticulum and mitochondria (MT). It was also shown that protein aggregates formed in the presence of different lipids exerted drastically different levels of endosomal damage.[23] Expanding upon this, we utilized the real-time polymerase chain reaction (rt-PCR) to determine changes in the expression of proteins that play a key role in the unfolded protein response (UPR) of N27 rat dopaminergic cells exposed to α-Syn fibrils formed in the presence of PC, CL, and Cho. We also performed rt-PCR analysis of changes in the expression of genes responsible for the MT response to unfolded proteins in such cells.

RESULTS AND DISCUSSION

Structural and Morphological Characterization of a-Syn Aggregates. In the lipid-free environment, α-Syn formed elongated fibril-like structures with a height range of 8−10 nm (Figure 1a,b). Similar morphological fibrils were observed in α-Syn:CL and α-Syn:PC:Cho samples with heights comparable to those formed in the lipid-free environment. However, in the presence of PC LUVs, a-Syn formed only small oligomers with a height of 2−3 nm. Fourier-transform Infrared (FTIR) reveals the predominance of parallel β-sheet secondary structure (1627 cm^{-1}) in α-Syn:CL, α-Syn:PC:Cho, and α-Syn samples (Figure 1c). On the other hand, the α-Syn:PC aggregates were found to be predominately composed of unordered secondary structure (1650 cm^{-1}). Similar results were found using circular dichroism (CD) spectroscopy (Figure 1d). Specifically, α-Syn fibrils grown in the presence of CL and PC:Cho, as well as in the lipid-free environment, exhibited a predominant parallel β-sheet secondary structure, whereas a-Syn:PC exhibited a predominance of unordered secondary structure. It should be noted that in the analyzed samples, a substantial amount of unaggregated protein could be present. At the same time, both CD and FTIR measurements measure the bulk

https://doi.org/10.1021/acschemneuro.3c00671
ACS Chem. Neurosci. XXXX, XXX, XXX−XXX

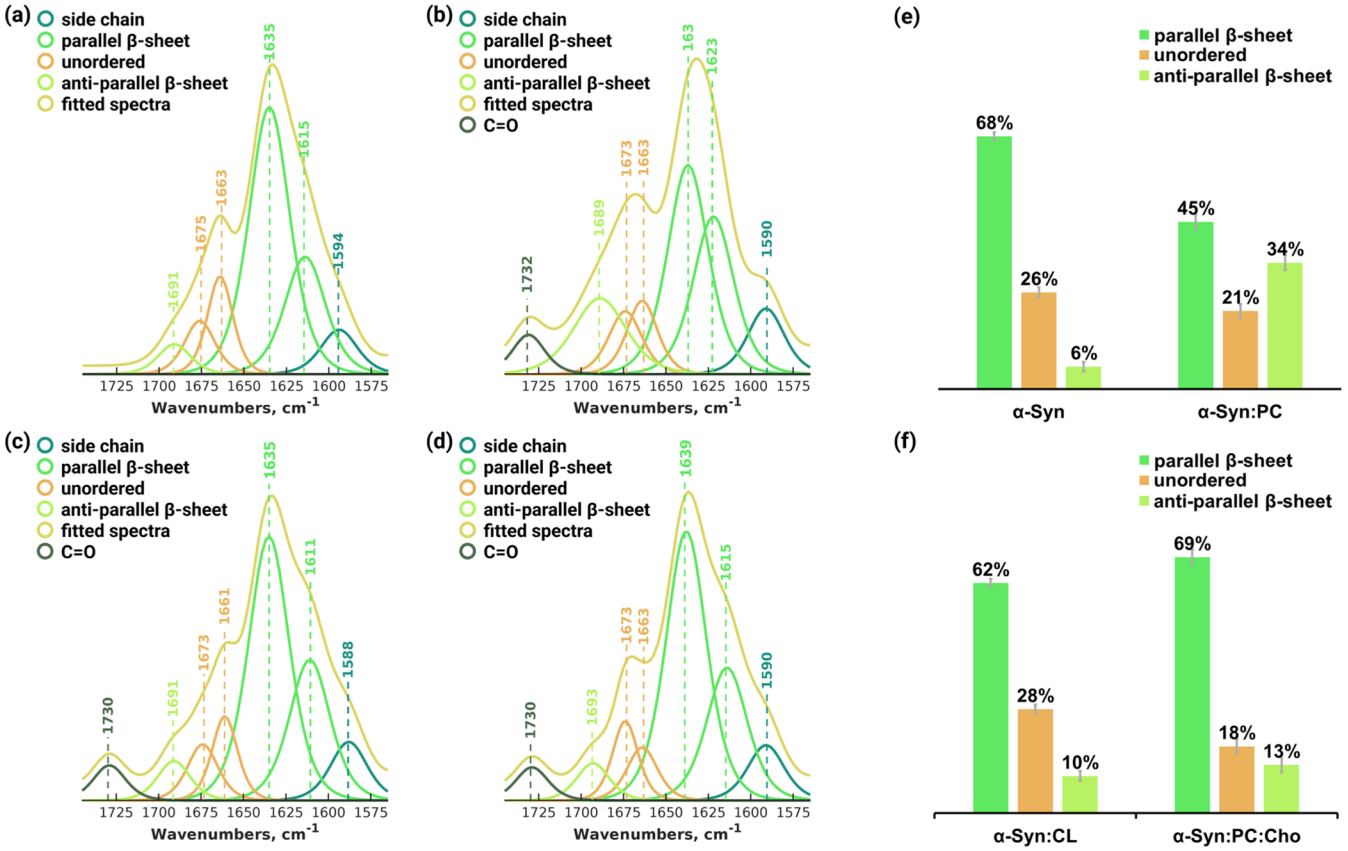

Figure 2. Averaged IR spectra of α-Syn (a), α-Syn:PC (b), α-Syn:CL (c), and α-Syn:PC:Cho (d) with the fitted protein secondary structures. Histograms (e, f) summarize the relative amount of parallel β-sheet, unordered protein, and antiparallel β-sheet in the analyzed protein aggregates.

Scheme 1. Schematic Illustration of UPR of ER Activated by Amyloid Aggregates

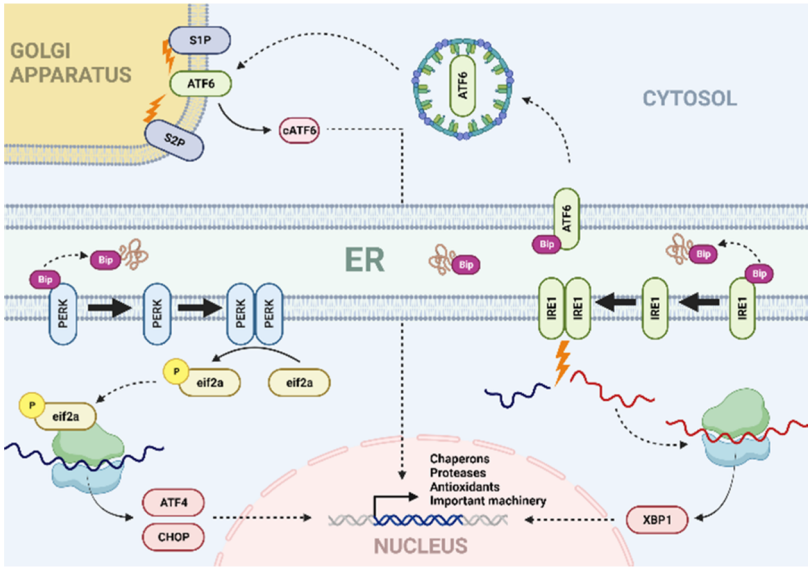

volume of the sample. Consequently, the presence of the monomeric α-Syn may alter the information about the secondary structure of the oligomers and fibrils present in such samples. To overcome this problem, we utilized atomic force microscopy Infrared (AFM-IR) spectroscopy. In AFM-IR, a metalized scanning probe can be positioned on the surface of individual oligomers and fibrils.[25−30] Pulsed tunable IR light used in AFM-IR, induces thermal expansions in these aggregates that are reordered by the scanning probe.[31−33] Next, the thermal expansions are converted into IR spectra that similar to FTIR spectra can be used to determine the secondary structure of individual amyloid oligomers and fibrils.[20,28,34−38]

AFM-IR revealed high similarities in the secondary structures of α-Syn and α-Syn:CL fibrils. We found that both fibrillar species were dominated by parallel β-sheet (62−68%)

https://doi.org/10.1021/acschemneuro.3c00671
ACS Chem. Neurosci. XXXX, XXX, XXX−XXX

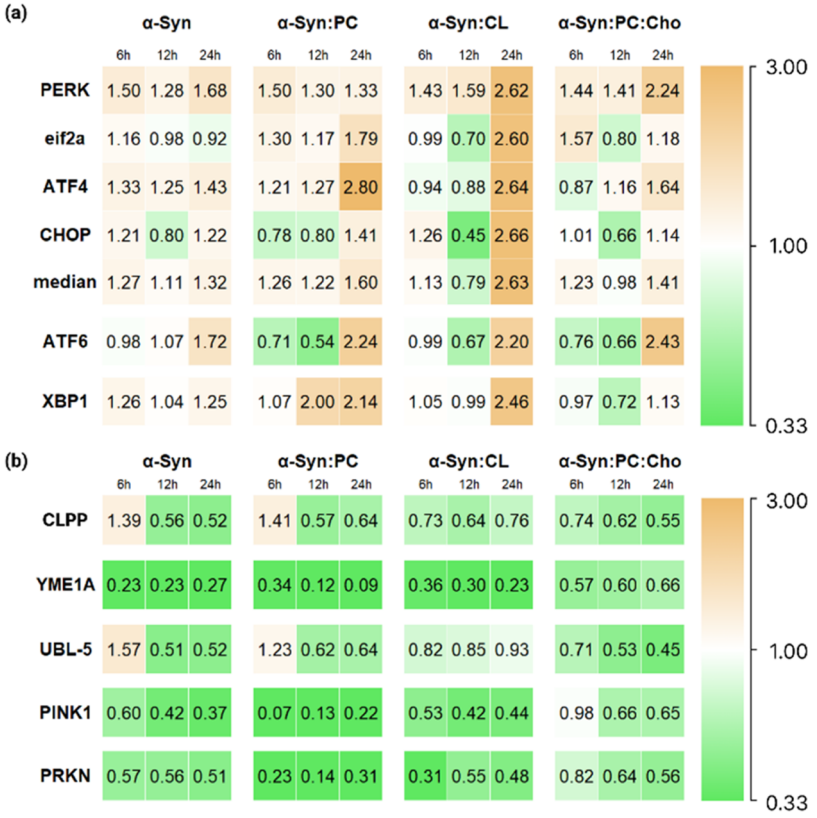

Figure 3. (a) Heat map of relatives UPR (a) and MT-UPR (b) gene expression as a result of the N27 cell exposure to α-Syn, α-Syn:PC, α-Syn:CL, and α-Syn:PC:Cho aggregates for 6, 12, and 24 h.

with ~27% of unordered protein secondary structure, Figure 2. Both α-Syn and α-Syn:CL fibrils had 6−10% of antiparallel β-sheet. α-Syn:PC:Cho fibrils have a much higher amount of parallel β-sheet (69%) than α-Syn:CL fibrils. These aggregates also possessed 18 and 13% unordered protein and antiparallel β-sheet, respectively. Using AFM-IR, we found that α-Syn:PC oligomers possessed 45 and 34% of parallel and antiparallel β-sheet, respectively. These oligomers also had ~21% unordered protein secondary structure. Finally, AFM-IR revealed the presence of carbonyl vibration of lipids (1732 cm^{-1}) in the IR spectra acquired from α-Syn:PC, α-Syn:CL, and α-Syn:PC:Cho that were not evident in the spectrum acquired form α-Syn fibrils.[18,19] These results indicated that lipids were present in the structure of the protein aggregates that formed in their presence.

Activation of Unfolded Protein Response (UPR) in Endoplasmic Reticulum (ER) Stress Induced by a-Syn. The UPR involves three transmembrane proteins: PERK (PKR-like ER kinase), IRE1 (Inositol Requiring 1), and ATF6 (Activating Transcription Factor 6), Scheme 1.[39−41] These proteins are regulated by GRP78 (78-kDa glucose-regulated chaperon), also known as BiP.[42,43] Activation of PERK, an ER transmembrane kinase, leads to autophosphorylation and subsequently triggers the expression of eukaryotic initiation factor 2 (eIF2a). eIF2a inhibits the assembly of ribosomal complexes involved in mRNA translation,[44−47] leading to reduced protein expression and minimizing the ER workload in the cell. Furthermore, eIF2a activates ATF4, a pro-apoptotic activating transcription factor, which, in turn, activates CHOP (C/EBP Homologous Protein). CHOP regulates the expression of caspase 3 kinase and members of the BCL2 protein family, Scheme 1.[48,49]

qPCR-based analysis revealed a slight increase in the levels of PERK expression in the cells exposed to α-Syn fibrils compared with the control. Specifically, at 6 h, we found a 1.5-fold increase in the expression of PERK that was followed by a slight decrease at 12 h (1.28-fold), Figure 3. At 24 h, a significant increase in PERK expression (1.68-fold) was observed. Similar changes in the expression of PERK were observed in the cells exposed to α-Syn:PC at 6 and 12 h. At the same time, PERK expression levels remained on the same level at 24 h (1.33-fold), which was not observed in the cells exposed to α-Syn fibrils. A strong and continuous upregulation of PERK expression was also observed in the N27 cells exposed to α-Syn:CL fibrils. At 6 h, the expression of PERK was 1.43-fold higher and then further increased to 1.59-fold and 2.62-fold at 12 and 24 h, respectively. Similar changes in PERK expression were observed in the cells exposed to the α-Syn:PC:Cho fibrils. Specifically, at 6 and 12 h, PERK expression was 1.44-fold and 1.41-fold higher compared with the control. Finally, at 24 h, PERK expression was further increased to 2.24-fold compared with the control.

We also observed an upregulation of the expression of eIF2α in the cells exposed to α-Syn fibrils. However, after a slight increase in the expression of eIF2α at 6 h (1.16-fold), we found a continuous decrease in the expression of this protein by 12 h (0.98-fold) and 24 h (0.92-fold), Figure 2. At the same time, a completely different behavior of eIF2α expression was observed in the cells exposed to α-Syn:PC. Specifically, we observed a continuous increase in the expression level of eIF2α from 6 (1.30-fold) to 24 h (1.79-fold). We also found no

https://doi.org/10.1021/acschemneuro.3c00671
ACS Chem. Neurosci. XXXX, XXX, XXX−XXX

Scheme 2. Schematic Illustration of UPR of MT Activated by the Unfolded Protein

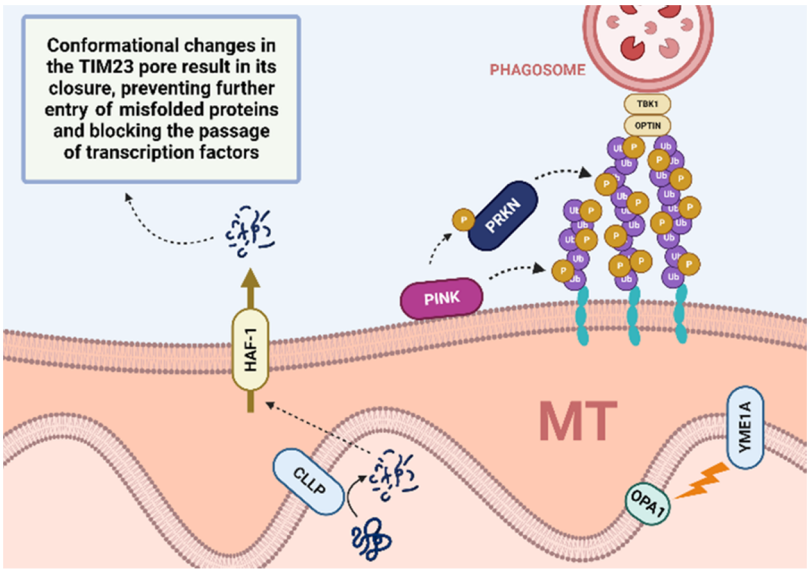

changes in the expression of eIF2α in the cells exposed to α-Syn:CL fibrils at 6 h which was followed by a suppression of eIF2α expression (0.7-fold decrease) at 12 h. However, a strong upregulation (2.6-fold) in the expression of eIF2α was observed in the cells exposed to α-Syn:CL fibrils for 24 h. In N27 cells exposed to α-Syn:PC:Cho fibrils, we observed first an increase in the expression of eIF2α (6 h) that was followed by a decrease at 12 h. Finally, we found a 1.18-fold increase in the level of expression of eIF2α in the cells exposed to α-Syn:PC:Cho fibrils.

Based on our results, a moderate increase in the expression of ATF4 in the cells exposed to α-Syn fibrils was observed. Furthermore, a 1.33-fold increase was found at 6 h which was followed by a slight decrease by 12 h (1.25-fold), Figure 2. After this time point, we observed an increase of 1.43-fold in the expression levels of ATF4 in the cells exposed to α-Syn fibrils by 24 h. In the cells exposed to α-Syn:PC aggregates, a continuous increase in the expression levels of ATF4 was observed from 6 (1.2-fold) to 24 h (2.8-fold). In the case of α-Syn:CL fibrils, we first observed a very small decrease in the expression of ATF4 at 6 and 12 h that was followed by a strong increase at 24 h. Our results also showed that α-Syn:PC:Cho fibrils caused a decrease in the expression of ATF4 at 6 h (0.87-fold) which was followed by a continuous increase at 12 and 24 h (1.16-fold and 1.64-fold, respectively).

α-Syn fibrils caused a slight increase in the expression of CHOP in N27 cells compared to that of the control. At 6 h, CHOP expression exhibited a modest elevation (1.21-fold), followed by a decrease at 12 h (0.80-fold), Figure 2. However, at 24 h, a 1.22-fold increase in CHOP expression was observed. In the cells exposed to α-Syn:PC aggregates, we first observed a decrease in the expression of CHOP at 6 and 12 h which was followed by a 1.41-fold increase by 24 h. We found that both α-Syn:CL and α-Syn:PC:Cho fibrils caused first an increase in CHOP expression levels (6 h) that were followed by a small decrease in the expression of this protein by 12 h. Finally, a strong increase in the expression of CHOP was observed in the cells exposed to both α-Syn:CL and α-Syn:PC:Cho fibrils after 24 h. These results demonstrate that α-Syn fibrils formed in the presence of PC, CL, and Cho caused drastically different changes in the URP response of the cells.

The ER stress leads to significant alterations in the expression of ATF6, a type II ER transmembrane transcription factor, Scheme 1. Following its expression, ATF6 moves to the Golgi apparatus, where it undergoes processing to generate an active transcription factor fragment, called cATF6. This cATF6 fragment plays a crucial role in mitigating the effects of ER stress.[42,43] In the cells exposed to α-Syn fibrils, we observed no significant changes in the levels of ATF6 expression in the first 12 h. However, a strong increase in the expression of ATF6 (1.72-fold) was observed at 24 h. In the case of α-Syn:PC and α-Syn:PC:Cho aggregates, we observed a strong suppression of ATF6 expression in the first 12 h. However, an even greater magnitude of the activation of ATF6 expression was observed at 24 h in the cells exposed to α-Syn:PC oligomers (2.24-fold) and α-Syn:PC:Cho fibrils (2.43-fold). Similar changes were observed in the cells exposed to the α-Syn:CL fibrils. We first observed no changes (6 h) in ATF6 expression that were followed by a small decrease in the expression of ATF6 (12 h). Finally, a drastic increase (2.2-fold) in ATF6 expression was observed by 24 h.

IRE1 is a type I ER transmembrane kinase that forms dimers and undergoes autophosphorylation in response to unfolded or misfolded proteins, Scheme 1.[47] Once activated, IRE1 performs splicing of X-box binding protein 1 (XBP-1) mRNA, as indicated in references.[44−46] The spliced XBP1 mRNA encodes a basic leucine zipper (b-ZIP) transcription factor, which plays a significant role in upregulating UPR target genes, as well as genes responsible for encoding folding proteins like protein disulfide isomerase and chaperones.[44−46] In the cells exposed to α-Syn fibrils, we found an increase in the expression of XBP1 at 6 h (1.26-fold) that was followed by a decrease in the expression of this protein by 12 h (1.04-fold). Similar to 6 h levels of XBP1 expression were observed in the cells exposed to α-Syn fibrils at 24 h (1.25-fold). We observed no substantial changes in the expression of XBP1 in the cells exposed to α-Syn:PC aggregates at 6 h. However, a strong increase in the XBP1 expression was observed in the cells at 12 h (2.0-fold) and 24 h (2.14-fold). Similar changes were observed in the level of XBP1 expression in the cells exposed to α-Syn:CL fibrils. However, we observed no changes in the XBP1 expression for the first 12 h, which were followed by a

https://doi.org/10.1021/acschemneuro.3c00671
ACS Chem. Neurosci. XXXX, XXX, XXX−XXX

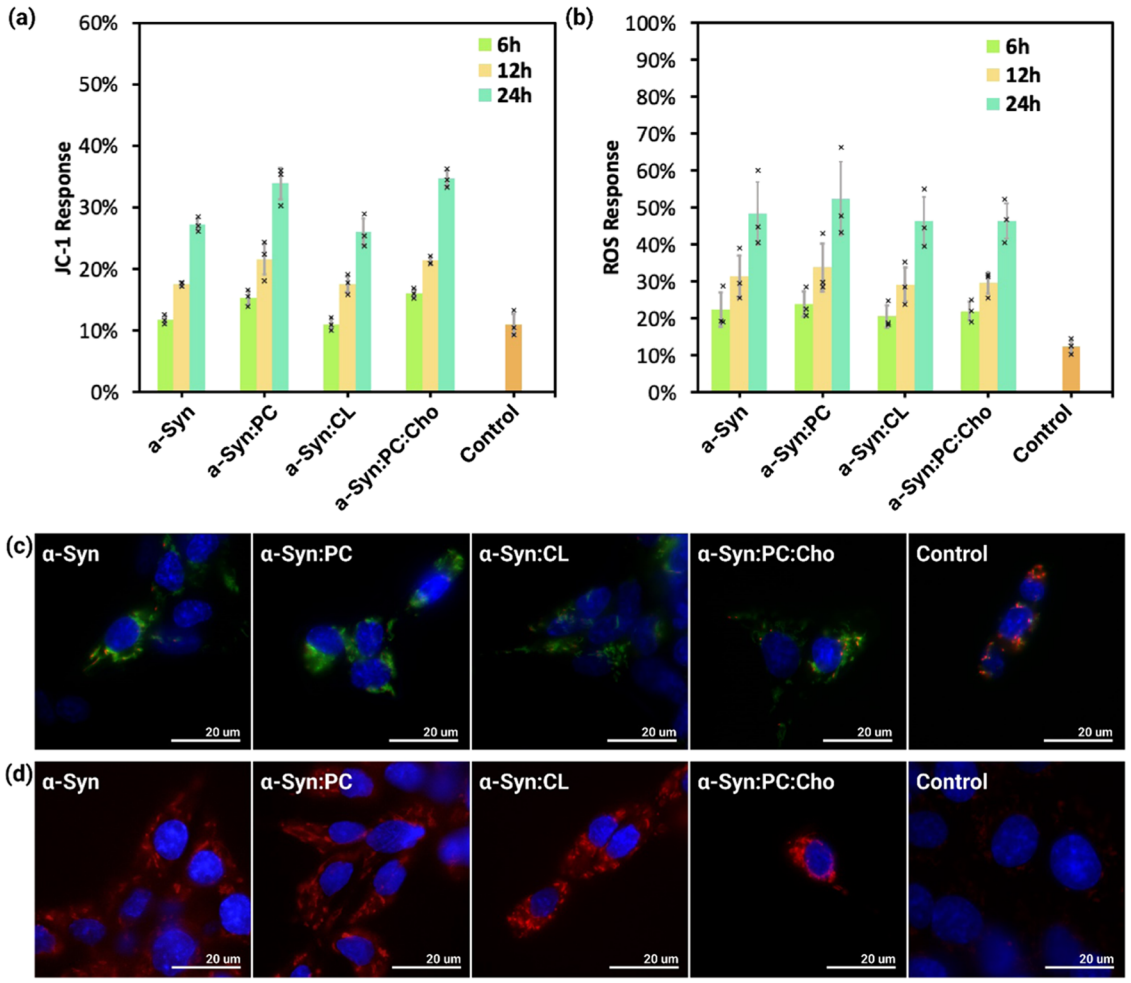

Figure 4. Histogram of JC-1 (a) and ROS (b) cytotoxicity assay of N27 cells were incubated for 6,12, and 24 h with a-Syn aggregates formed in the presence of PC, CL, and PC:Cho LUVs, as well as in a lipid-free environment. Fluorescence microscopy images that show JC-1 monomer (green) and JC-1 polymer (red) (c) and ROS response (red) (d) fluorescence for treated N27 cells for 24 h with protein aggregates for 96 h. The blue fluorescence represents the nuclear fluorescence dye.

strong 2.46-fold increase at 24 h. In the cells exposed to α-Syn:PC:Cho fibrils, we observed no changes in the XBP1 expression at 6 h. Next, a small suppression of XBP1 expression was observed at 12 h which was followed by an increase to 1.13-fold at 24 h. These results further confirmed that α-Syn fibrils formed in the presence of PC, CL, and Cho caused drastically different changes in the URP responses of the cells.

MT-UPR Activation in Response to Stress Induced by α-Syn Aggregates. Within MT, the unfolded protein response (MT-UPR) serves as an essential cellular mechanism responsible for maintaining adequate protein folding. This intricate process relies on the involvement of several pivotal proteins, namely, CLPP, YME1A, UBL-5, PINK1, and PRKN. Each of these proteins plays an important role in orchestrating the cellular response to UPR activation. These proteins also contribute to the proper organization and execution of MT-UPR, ensuring the maintenance of mitochondrial protein homeostasis and cellular function.

CLPP is an essential protease enzyme located in the mitochondrial matrix (MT matrix). Its primary role is to facilitate the degradation of misfolded or damaged proteins, thereby preventing their buildup and potentially harmful effects. Through selective cleavage of these abnormal proteins, CLPP plays a crucial role in preserving the homeostasis of mitochondrial proteins, Scheme 2.[50] In the cells exposed to α-Syn fibrils and α-Syn:PC oligomers, we observed first an upregulation of CLLP expression at 6 h (1.39-fold and 1.41-fold, respectively) that was followed by a decrease in CLPP gene expression by 0.56-fold and 0.52-fold, respectively, for α-Syn fibrils and 0.57-fold and 0.64-fold for α-Syn:PC oligomers. We also found that α-Syn:CL and α-Syn:PC:Cho fibrils exerted similar downregulation responses of CLLP that ranged from 0.55-fold to 0.76-fold at different time points after the exposition of the cells to the protein aggregates.

YME1A is a significant mitochondrial protease involved in the MT-UPR response. It is responsible for targeting and degrading unfolded or misfolded proteins located in the inner MT membrane space. By recognizing and eliminating damaged proteins, YME1A plays a crucial role in maintaining MT protein quality control, thereby safeguarding the proper functioning of mitochondria.[51] We observed a strong down-regulation of YME1A expression in the cells exposed to α-Syn fibrils from 0.23-fold at 6 h to 0.27-fold at 24 h. Even stronger suppression of YME1A expression was observed in the cells exposed to α-Syn:PC oligomers. We found that the expression of this protein changed from 0.34-fold at 6 h to 0.09-fold by 24 h. A similar magnitude of the suppression of YME1A

https://doi.org/10.1021/acschemneuro.3c00671
ACS Chem. Neurosci. XXXX, XXX, XXX−XXX

expression was observed in the cells exposed to α-Syn:CL and α-Syn:PC:Cho. Specifically, in the case of α-Syn:CL the expression decreased from 0.36-fold (6 h) to 0.23-fold (24 h), whereas in the case of α-Syn:PC:Cho, the expression of YME1A changed from 0.57-fold (6 h) to 0.66-fold (24 h).

Ubiquitin-like protein 5 (UBL-5) plays a crucial role in clearing damaged or unfolded proteins. As a nuclear protein, it functions as a transcriptional regulator, controlling the expression of genes related to mitochondrial protein folding, degradation, and dynamics, thereby contributing to proper mitochondrial protein maintenance.[52] Although at 6 h after cell exposure to both α-Syn and α-Syn:PC the expression of UBL-5 increased 1.57- and 1.23-fold, respectively, we observed a strong suppression of this gene expression during the next 24 h. Specifically, in the case of α-Syn, the expression decelerated ∼0.5-fold at 12 and 24 h, whereas in the case of α-Syn:PC, ∼0.6-fold suppression of UBL-5 expression was observed. In the cells exposed to α-Syn:CL, we observed a strong suppression of UBL-5 expression at all time points. A similar cell response was observed in the case of α-Syn:PC:Cho. We observed 0.71-fold suppression at 6, h, which was followed by 0.53-fold and 0.45-fold downregulation of UBL-5 expression at 12 and 24 h.

PTEN-induced kinase 1 (PINK1) and PRKN (Parkin) are two essential kinases responsible for upholding the integrity of the mitochondrial unfolded protein response (MT-UPR). PINK1 acts as a sensor for mitochondrial dysfunction, specifically in the cases of MT-UPR and membrane damage, leading to its accumulation on the outer surface of mitochondrial membranes. Through autophosphorylation, PINK1 activates PRKN, which, in turn, plays a crucial role in regulating the process of mitophagy, targeting and removing damaged mitochondria from the cell. We observed a strong suppression of both PINK1 and PRKN in the cells exposed to all protein aggregates. Specifically, in the case of α-Syn fibrils, we found a 0.6-fold suppression of PINK1 at 6 h that was followed by 0.42-fold and 0.37-fold suppression at 12 and 24 h. At the same time, 0.6-fold suppression of PRKN was observed throughout 24 h of exposure of the cell to α-Syn fibrils. The even greater magnitude of suppression (0.31−0.07-fold) of both PINK1 and PRKN were observed for α-Syn:PC. We also found a propagating increase in the suppression of both PINK1 and PRKN in the case of α-Syn:PC:Cho that changed from 0.98- and 0.82-fold, respectively, at 6 h to ∼0.6-fold at 24 h. Finally, in the cells exposed to α-Syn:CL, we observed 0.53- and 0.31-fold suppression of both PINK1 and PRKN, respectively, at 6 h. At 24 h, both PINK1 and PRKN were ∼0.4-fold downregulated compared to the control.

External vs Internal Impairment of MT Caused by α-Syn Aggregates Formed in the Presence and Absence of LUVs. We employed JC-1 assay to investigate the dynamics of mitochondrial impairment caused by α-Syn fibrils formed in the presence and absence of LUVs at 6, 12, and 24 h after the exposure of N27 rat dopaminergic cells to the protein aggregates, Figure 4(a).

In the cells exposed to α-Syn fibrils, JC-1 showed a continuous increase in the magnitude of mitochondrial impairment. At 6, 12, and 24 h, the percentages of JC-1 response were 11.77 ± 0.61, 17.57 ± 0.32, and 27.23 ± 0.99%, respectively, Figure 4. Similar changes in the JC-1 response were observed in the cells exposed to α-Syn:PC oligomers and α-Syn:CL fibrils. In the case of α-Syn:PC, at 6, 12, and 24 h, the percentages of JC-1 response were 15.35 ± 1.09, 20.93 ± 1.96, and 33.89 ± 2.58%, respectively. In the case of α-Syn:CL, at 6, 12, and 24 h, the percentages of JC-1 response were 11.02 ± 0.89, 17.6 ± 1.3, and 26.03 ± 2.16%, respectively. We also observed a consistent increase in the JC-1 response over time in the cells exposed to α-Syn:PC:Cho. At 6, 12, and 24 h, the percentages of JC-1 response were 16.05% ± 0.63, 21.37 ± 0.56, and 34.67 ± 1.26%, respectively. At the same time, control cells exhibited a relatively stable JC-1 response throughout the experimental period, with a percentage of 11.03 ± 1.68%, Figure 4.

We performed fluorescence imaging of N27 cells exposed to α-Syn, α-Syn:PC, α-Syn:CL, and α-Syn:PC:Cho for 24 h, Figure 4(c). Microscopic analysis of the cells showed a significant increase in green JC-1 fluorescence intensity in the cells exposed to all protein aggregates compared to that of the control cells.

Reactive oxygen species (ROS) assay was used to quantify the magnitude of ROS in N27 cells after exposure to α-Syn, α-Syn:PC, α-Syn:CL, and α-Syn:PC:Cho, Figure 4. The Deep Red fluorescent dye, used in the ROS assay, is permeable to live cells and able to detect superoxide and hydroxyl radicals, two key ROS indicators. Upon entering the cell, the dye is oxidized by ROS to produce a bright fluorescent signal that can be measured using flow cytometry or detected by fluorescence imaging. In the cells exposed to α-Syn fibrils, we observed a continuous increase in ROS throughout the experiment. Specifically, at 6, 12, and 24 h, the percentages of ROS response were 22.38 ± 4.58, 31.38 ± 5.68, and 48.46 ± 8.42%, respectively, Figure 4. Similarly, the α-Syn:PC-treated cells exhibited a gradual increase in the ROS over time. At 6, 12, and 24 h, the percentages of ROS response were 23.89 ± 3.33, 33.84 ± 6.54, and 52.41 ± 9.98%, respectively. In the α-Syn:CL treatment group, the ROS response also showed a progressive increase with time. At 6, 12, and 24 h, the percentages of ROS response were 20.58 ± 3, 29.19 ± 4.72, and 46.43 ± 6.47%, respectively. Furthermore, the α-Syn:PC:Cho treatment group demonstrated a consistent rise in the ROS response over time. At 6, 12, and 24 h, the percentages of ROS response were 22.05 ± 2.45, 29.59 ± 2.84, and 46.54 ± 4.76%, respectively. In contrast, the control group exhibited relatively stable levels of ROS response throughout the experimental period. At 6, 12, and 24 h, the percentages of ROS response were consistently 12.38 ± 1.73%, Figure 4(b).

Furthermore, fluorescence microscopy analysis was conducted on N27 cells exposed to α-Syn aggregates in the presence and absence of PC, CL, and PC:Cho LUVs for a duration of 24 h (Figure 4(d)). The images clearly revealed a notable enhancement in ROS fluorescence intensity within cells treated with different protein aggregates, when compared to the control cells.

DISCUSSION

A growing body of experimental evidence indicates that the toxicity of amyloid oligomers and fibrils can be altered by lipids present at the stage of protein aggregation.[18−21,53−56] Atomic force microscopy Infrared (AFM-IR) spectroscopy revealed that such aggregates had drastically different secondary structures.[18−21,53−56] For instance, insulin oligomers formed in the presence of PC primarily possessed unordered protein secondary structure, whereas insulin fibrils that were formed in the presence of CL, on the opposite, were primarily composed of parallel β-sheet.[23,56] AFM-IR also showed that such aggregates possessed lipids in their structure. Specifically, α-

https://doi.org/10.1021/acschemneuro.3c00671
ACS Chem. Neurosci. XXXX, XXX, XXX−XXX

Syn oligomers were formed in the presence of PC and PS exhibited the vibrational signatures of these phospholipids.[18,19] These findings indicated that both changes in the protein secondary structure and the presence of lipids can be considered the key determinants of oligomer and fibril toxicity.

Experimental findings reported in this study showed that α-Syn oligomers and fibrils formed in the presence of PC, CL, and PC:Cho exerted drastically different magnitudes of UPR in N27 rat dopaminergic cells. We also found that not only the magnitude but also dynamics of the UPR were different for α-Syn, α-Syn:PC, α-Syn:CL, and α-Syn:PC:Cho. Although primarily upregulation of the expression of UPR-related proteins was observed, we found primarily downregulation of the expression of proteins responsible for MT-UPR. However, when we examined the effects of individual lipids on gene expression, our experiments showed a key distinction: isolated lipids do not significantly alter UPR and MT-UPR gene expression (Figure S3). One can expect that in the event of mitochondrial dysfunction, activated MT-UPR increases the production of ATP.[57] Thus, suppressed MT-UPR can be indicative of detrimental processes that take place in mitochondria as a result of cell exposure to amyloid aggregates. These results also indicate that mechanisms that determine the toxicity of amyloid oligomers and fibrils are fairly complex and likely to involve numerous cell signaling pathways that are yet to be determined.

METHODS

Preparation of Large Unilamellar Vesicles (LUVs). Avanti Polar Lipids (Alabaster, AL) provided 1,2-dimyristoyl-sn-glycero-3-phosphocholine (14:0 PC (PC)) (Cat. No. 850345), 18:00 cardiolipin (CL) (Cat. No. 710334), and cholesterol (Chol) (Cat. No. 700100). To create LUVs, PC, and CL were dissolved in 1× PBS with a pH of 7.4, reaching a final concentration of 400 μM. For the 5:95 mol/mol Chol:PC mixture, PC and Chol were initially mixed in chloroform at a 5:95 molar ratio. Next, chloroform was evaporated under a dry N_2 stream until a lipid film was formed. The film was dissolved in 1× PBS at pH 7.4. All samples underwent five freeze−thaw cycles using liquid nitrogen and a hot water bath to ensure uniformity and stability. Finally, the lipid solutions were extruded with a LIPEX Flow Extruder equipped with a 100 nm membrane (A.M.D. Manufacturing Inc. Cat. No. AMDPCTE010025C) to produce LUVs with an approximate diameter of 100 nm, confirmed by dynamic light scattering (DLS), Figure S1.

Protein Expression and Purification α-Syn. The pET21a-α-synuclein plasmid was transformed into an *Escherichia coli* BL21 (DE3) Rosetta strain, and the bacteria were grown in LB broth media according to the protocol described by Volles and Lansbury. After reaching an appropriate cell density, protein expression was induced by adding 1 mM IPTG. Two liters of the bacterial culture were pelleted down by centrifugation at 8000 rpm for 10 min. The resulting cell pellet was collected. The cell pellet was resuspended in lysis-tris buffer (50 mM Tris, 10 mM EDTA, and 150 mM NaCl, pH 7.5). The suspended cells were then boiled in a water bath for 30 min to lyse the cells and release the expressed proteins. The lysed samples were centrifuged at 16,000*g* for 40 min. This step helped to separate the cellular debris from the soluble proteins. The supernatant containing the soluble proteins was collected. To precipitate unwanted proteins and contaminants, streptomycin sulfate (10% solution, 136 μL/mL) and glacial acetic acid (228 μL/mL) were added to the supernatant. The mixture was then centrifuged at 16,000*g* for 10 min at 4 °C. The resulting supernatant was precipitated by adding an equal volume of saturated ammonium sulfate at 4 °C. The mixture was centrifuged to collect the protein precipitate. The protein pellet obtained from ammonium sulfate precipitation was washed with a $(NH_4)_2SO_4$ solution at 4 °C (a 1:1 v/v mixture of saturated ammonium sulfate and water). This step was performed to remove residual contaminants and salts. The washed protein pellet was resuspended using 100 mM $NH_4(CH_3COO)$ under constant stirring for 5 min. To further purify the protein, an equal volume of absolute ethanol was added to the resuspended protein solution. The mixture was then subjected to ethanol precipitation. This step was repeated twice at room temperature and collect the purified pellets. Pellets were dissolved in the PBS buffer.

Size Exclusion Chromatography (SEC). The protein pellet was dissolved in PBS buffer, pH 7.4. The solution was centrifuged for 30 min at 14,000*g* using a benchtop microcentrifuge (Eppendorf centrifuge 5424). Next, 500 μL of the concentrated α-syn was loaded onto a Superdex 200 10/300 gel filtration column installed in an AKTA pure (GE Healthcare) FPLC system. Proteins were eluted isocratically using the same buffer (PBS, pH 7.4) at a flow rate of 0.5 mL/min at 4 °C. During the FPLC run, 1.5 mL fractions were collected based on ultraviolet−visible (UV−vis) detection at 280 nm.

Protein Aggregation. α-Syn was dissolved in 1× PBS, pH 7.4, to reach the final concentrations of 60 μM. In parallel, α-syn was mixed with LUVs to reach the final concentration of LUVs of 240 μM (1:4 protein:lipid ratio). Samples were incubated at 37 °C under addition at 510 rpm for 98 h.

Atomic Force Microscopy (AFM). A 5 μL aliquot of the sample was placed on silicon wafers for 3 min. Subsequently, the wafers were gently rinsed with deionized water and dried using N_2 gas. AFM imaging was performed using a Nano-IR 3 system (Bruker, Santa Barbara, CA) equipped with a QCL laser. Contact-mode AFM tips (ContGB-G AFM probe, NanoAndMore) were used for image acquisition.

Circular Dichroism (CD). CD spectra were recorded at 25 °C by using a J-1000 CD spectrometer (Jasco, Easton, MD). Each sample was measured in triplicate over the 195−240 nm wavelength range.

Attenuated Total Reflectance Fourier-Transform Infrared (ATR-FTIR) Spectroscopy. A 2 μL aliquot of the sample was deposited onto an ATR crystal and allowed to air-dry at room temperature. FTIR spectra were collected using a Spectrum 100 FTIR spectrometer (PerkinElmer, Waltham, MA), with three spectra acquired from each sample.

Cell Toxicity Assays. N27 rat dopaminergic neuron cells were cultured in RPMI 1640 medium (Thermo Fisher Scientific) supplemented with 10% fetal bovine serum (FBS) (Invitrogen, Waltham, MA) in a 48-well plate, with 30,000 cells per well. The cells were maintained at 37 °C with 5% CO_2. After 24 h, when the cells adhered completely to the wells, 300 μL of the cell culture medium was replaced with 300 μL of RPMI 1640 Medium containing 5% FBS and 30 μL of protein samples to achieve final protein and lipid concentration 6 and 24 μM, respectively. Following a 6, 12, and 24 h incubation period, a reactive oxygen species (ROS) assay was performed. The ROS reagent (C10422, Invitrogen) was added to achieve a final concentration of 5 μM. Cells were then incubated at 37 °C in a 5% CO_2 environment for 30 min. After the supernatant was removed, cells were washed with RPMI 1640 media supplemented with 5% FBS, treated with trypsin, and suspended in 200 μL of 1× PBS at pH 7.4. Sample measurements were conducted using the red channel (λ = 633 nm) of an Accuri C6 Flow Cytometer (BD, San Jose, CA). The percentage of ROS-positive cells was determined by using Acura software. For JC-1 staining, JC-1 reagent (M34152A, Invitrogen) was added to the cells to achieve a final concentration of 50 μM and incubated at 37 °C in a 5% CO_2 environment for 30 min. After the supernatant was removed and the cells were treated with trypsin, they were resuspended in 200 μL of 1× PBS at pH 7.4. Sample measurements were obtained using the green channel (λ = 488 nm) of an Accuri C6 Flow Cytometer (BD, San Jose, CA). The percentage of cells exhibiting JC-1 staining was determined accordingly.

Fluorescence Microscopy. N27 rat dopaminergic neuron cells were cultured in RPMI 1640 Medium (Thermo Fisher Scientific) supplemented with 10% fetal bovine serum (FBS) (Invitrogen, Waltham, MA) in 35 mm dishes with optical bottoms (Cat. No. D35−10−1.5-N, Cellvis), with 300,000 cells per well, and maintained at 37 °C in a 5% CO_2 environment. After 24 h, when the cells fully

https://doi.org/10.1021/acschemneuro.3c00671
ACS Chem. Neurosci. XXXX, XXX, XXX−XXX

adhered to the wells, the cell culture medium was replaced with fresh RPMI 1640 Medium containing 5% FBS and including the protein samples. After 6, 12, and 24 h of incubation, ROS and JC-1 reagents were added to achieve final concentrations of 5 and 50 μM, respectively. Cells were incubated for 20 min at 37 °C in a 5% CO_2. Finally, 1 drop of NucBlue Live Cell ReadyProbes (Cat. No. R37605, Invitrogen) was added to each sample and incubated for 5 min at 37 °C in a 5% CO_2. Fluorescence images were captured using an EVOS M5000 Imaging System (Invitrogen) with an Olympus UPIanApo 100x/1.35 oil iris ∞/0.17 objective and blue, deep red, and green filters.

Gene Expression. RNA was extracted from the treated cells using a GeneJET RNA Purification Kit (catalog no. K0732, Thermo Scientific). The concentration of extracted RNA was determined using a NanoDrop One instrument (Thermo Scientific). cDNA synthesis was performed using SuperScript III Reverse Transcriptase (catalog no. 18080093, Invitrogen) with random primers (catalog no. 48190011, Invitrogen). Specific primers were designed for each target gene (refer to Table S1). The primer sequences were designed to be specific for the target genes and to be compatible with qPCR amplification conditions. qPCR reactions were carried out using a C1000 Touch Thermal Cycler (BioRad). Each reaction mixture contained a cDNA template, gene-specific primers, and SYBR Green PCR master mix (Cat. No. 4309155, Applied Biosystems). PCRs were performed in 35−40 cycles. β-actin was used as a housekeeping gene to normalize the expression levels of the target genes. Nontemplate controls and positive controls were included in each qPCR run to ensure the accuracy and reliability of the results.

Data Analysis. The quantification of relative gene expression was determined using the comparative Ct method ($2^{-\Delta\Delta Ct}$), where ΔCt represents the difference in threshold cycles between the target gene and the housekeeping gene and ΔΔCt represents the difference in ΔCt values between the treated samples and the control samples. The relative gene expression levels were calculated and presented as fold changes compared with the control samples.

CONCLUSIONS

We found that α-Syn oligomers and fibrils formed in the presence of lipids and a lipid-free environment triggered a strong UPR in N27 rat dopaminergic cells. The magnitude and dynamics of the ER stress within 6 to 24 h were substantially different for α-Syn, α-Syn:PC, α-Syn:CL, and α-Syn:PC:Cho. One can expect that both lipids present in such aggregates, as well as their secondary structure, uniquely alter the degree of ER damage in the dopaminergic cells. We also found that ER stress was linked to the strong suppression of the expression of genes that control MT-UPR. These findings suggested that aiming to overcome the ER stress, cells maximize mitochondrial activity. However, progressive failure to suppress the UPR-driven ER stress caused by amyloid aggregates ultimately leads to cell death. Thus, although substantial changes in mitochondrial activity are linked to amyloid-induced toxicity, they are likely to be the consequence of much more severe processes that take place in stressed neurons.

ASSOCIATED CONTENT

Supporting Information

The Supporting Information is available free of charge at https://pubs.acs.org/doi/10.1021/acschemneuro.3c00671.

Demonstrates the size profile of LUVs used in the study (Figure S1); summarizes the results of JC-1 and ROS experiments that investigated the cytotoxicity of lipids (Figure S2); heat map of relatives UPR and MT-UPR genes expression as a result of the N27 cell exposure to PC, CL, and Cho LUVs for 6, 12, and 24 h (Figure S3); summarizes the primer sequences used for qPCR analysis of changes in the expression of UPR and MT-UPR genes (Table S1) (PDF)

AUTHOR INFORMATION

Corresponding Author

Dmitry Kurouski − *Department of Biochemistry and Biophysics, Texas A&M University, College Station, Texas 77843, United States; Department of Biomedical Engineering, Texas A&M University, College Station, Texas 77843, United States;* orcid.org/0000-0002-6040-4213; Phone: 979-458-3778; Email: dkurouski@tamu.edu

Authors

Kiryl Zhaliazka − *Department of Biochemistry and Biophysics, Texas A&M University, College Station, Texas 77843, United States*

Abid Ali − *Department of Biochemistry and Biophysics, Texas A&M University, College Station, Texas 77843, United States*

Complete contact information is available at: https://pubs.acs.org/10.1021/acschemneuro.3c00671

Author Contributions

K.Z. conceptualized the study, performed all measurements, analyzed the data, and wrote and edited the manuscript. A.A. expressed and purified the protein and edited the manuscript. D.K. conceptualized the study, supervised the team, and wrote and edited the manuscript.

Notes

The authors declare no competing financial interest.

ACKNOWLEDGMENTS

We are grateful to the National Institute of Health for the provided financial support (R35GM142869).

REFERENCES

(1) Hawkes, C. H.; Del Tredici, K.; Braak, H. Parkinson's disease: a dual-hit hypothesis. *Neuropathol. Appl. Neurobiol.* **2007**, *33* (6), 599−614.

(2) Braak, H.; Del Tredici, K.; Rub, U.; de Vos, R. A.; Steur, E. N. H. J.; Braak, E. Staging of brain pathology related to sporadic Parkinson's disease. *Neurobiol. Aging* **2003**, *24* (2), 197−211, DOI: 10.1016/s0197-4580(02)00065-9.

(3) Braak, H.; Ghebremedhin, E.; Rub, U.; Bratzke, H.; Del Tredici, K. Stages in the development of Parkinson's disease-related pathology. *Cell Tissue Res.* **2004**, *318* (1), 121−134.

(4) Chen, J. Parkinson's disease: health-related quality of life, economic cost, and implications of early treatment. *Am. J. Managed Care* **2010**, *16*, S87−S93.

(5) Davie, C. A. A review of Parkinson's disease. *Br. Med. Bull.* **2008**, *86*, 109−127.

(6) Harris, M. K.; Shneyder, N.; Borazanci, A.; Korniychuk, E.; Kelley, R. E.; Minagar, A. Movement disorders. *Med. Clin. North Am.* **2009**, *93* (2), 371−388.

(7) Krack, P.; Volkmann, J.; Tinkhauser, G.; Deuschl, G. Deep brain stimulation in movement disorders: from experimental surgery to evidence-based therapy. *Mov. Disord.* **2019**, *34*, 1795−1810.

(8) Pieri, L.; Madiona, K.; Melki, R. Structural and functional properties of prefibrillar α-synuclein oligomers. *Sci. Rep.* **2016**, *6*, No. 24526, DOI: 10.1038/srep24526.

(9) Chen, S. W.; Drakulic, S.; Deas, E.; Ouberai, M.; Aprile, F. A.; Arranz, R.; Ness, S.; Roodveldt, C.; Guilliams, T.; De-Genst, E. J.; et al. Structural characterization of toxic oligomers that are kinetically trapped during alpha-synuclein fibril formation. *Proc. Natl. Acad. Sci. U.S.A.* **2015**, *112* (16), E1994−2003.

(10) Cremades, N.; Cohen, S. I.; Deas, E.; Abramov, A. Y.; Chen, A. Y.; Orte, A.; Sandal, M.; Clarke, R. W.; Dunne, P.; Aprile, F. A.; et al. Direct observation of the interconversion of normal and toxic forms of alpha-synuclein. *Cell* **2012**, *149* (5), 1048−1059.
(11) Apetri, M. M.; Maiti, N. C.; Zagorski, M. G.; Carey, P. R.; Anderson, V. E. Secondary structure of alpha-synuclein oligomers: characterization by raman and atomic force microscopy. *J. Mol. Biol.* **2006**, *355* (1), 63−71.
(12) O'Leary, E. I.; Lee, J. C. Interplay between alpha-synuclein amyloid formation and membrane structure. *Biochim. Biophys. Acta, Proteins Proteomics* **2019**, *1867* (5), 483−491.
(13) Kurouski, D.; Van Duyne, R. P.; Lednev, I. K. Exploring the structure and formation mechanism of amyloid fibrils by Raman spectroscopy: a review. *Analyst* **2015**, *140* (15), 4967−4980.
(14) Hong, D. P.; Han, S.; Fink, A. L.; Uversky, V. N. Characterization of the non-fibrillar alpha-synuclein oligomers. *Protein Pept. Lett.* **2011**, *18* (3), 230−240, DOI: 10.2174/092986611794578332.
(15) Galvagnion, C. The Role of Lipids Interacting with α-Synuclein in the Pathogenesis of Parkinson's Disease. *J. Parkinson's Dis.* **2017**, *7*, 433−450, DOI: 10.3233/jpd-171103.
(16) Galvagnion, C.; Brown, J. W. P.; Ouberai, M. M.; Flagmeier, P.; Vendruscolo, M.; Buell, A. K.; Sparr, E.; Dobson, C. M. Chemical properties of lipids strongly affect the kinetics of the membrane-induced aggregation of alpha-synuclein. *Proc. Natl. Acad. Sci. U.S.A.* **2016**, *113* (26), 7065−7070, DOI: 10.1073/pnas.1601899113.
(17) Galvagnion, C.; Buell, A. K.; Meisl, G.; Michaels, T. C.; Vendruscolo, M.; Knowles, T. P.; Dobson, C. M. Lipid vesicles trigger alpha-synuclein aggregation by stimulating primary nucleation. *Nat. Chem. Biol.* **2015**, *11* (3), 229−234.
(18) Dou, T.; Kurouski, D. Phosphatidylcholine and Phosphatidylserine Uniquely Modify the Secondary Structure of alpha-Synuclein Oligomers Formed in Their Presence at the Early Stages of Protein Aggregation. *ACS Chem. Neurosci.* **2022**, *13* (16), 2380−2385.
(19) Dou, T.; Zhou, L.; Kurouski, D. Unravelling the Structural Organization of Individual alpha-Synuclein Oligomers Grown in the Presence of Phospholipids. *J. Phys. Chem. Lett.* **2021**, *12* (18), 4407−4414.
(20) Zhaliazka, K.; Matveyenka, M.; Kurouski, D. Lipids Uniquely Alter the Secondary Structure and Toxicity of Amyloid beta 1−42 Aggregates. *FEBS J.* **2023**, *290* (12), 3203−3220.
(21) Zhaliazka, K.; Rizevsky, S.; Matveyenka, M.; Serada, V.; Kurouski, D. Charge of Phospholipids Determines the Rate of Lysozyme Aggregation but Not the Structure and Toxicity of Amyloid Aggregates. *J. Phys. Chem. Lett.* **2022**, *13* (38), 8833−8839.
(22) Matveyenka, M.; Rizevsky, S.; Kurouski, D. Elucidation of the Effect of Phospholipid Charge on the Rate of Insulin Aggregation and Structure and Toxicity of Amyloid Fibrils. *ACS Omega* **2023**, *8* (13), 12379−12386.
(23) Matveyenka, M.; Rizevsky, S.; Pellois, J. P.; Kurouski, D. Lipids uniquely alter rates of insulin aggregation and lower toxicity of amyloid aggregates. *Biochim. Biophys. Acta, Mol. Cell Biol. Lipids* **2023**, *1868* (1), No. 159247.
(24) Matveyenka, M.; Zhaliazka, K.; Rizevsky, S.; Kurouski, D. Lipids uniquely alter secondary structure and toxicity of lysozyme aggregates. *FASEB J.* **2022**, *36* (10), No. e22543.
(25) Dazzi, A. PhotoThermal Induced Resonance. Application to Infrared Spectromicroscopy. In *Thermal Nanosystems and Nanomaterials*; Volz, S., Ed.; Springer, 2009; Vol. *118*, pp 469−503.
(26) Dou, T.; Li, Z.; Zhang, J.; Evilevitch, A.; Kurouski, D. Nanoscale Structural Characterization of Individual Viral Particles Using Atomic Force Microscopy Infrared Spectroscopy (AFM-IR) and Tip-Enhanced Raman Spectroscopy (TERS). *Anal. Chem.* **2020**, *92* (16), 11297−11304.
(27) Ramer, G.; Ruggeri, F. S.; Levin, A.; Knowles, T. P. J.; Centrone, A. Determination of Polypeptide Conformation with Nanoscale Resolution in Water. *ACS Nano* **2018**, *12* (7), 6612−6619.
(28) Ruggeri, F. S.; Flagmeier, P.; Kumita, J. R.; Meisl, G.; Chirgadze, D. Y.; Bongiovanni, M. N.; Knowles, T. P. J.; Dobson, C. M. The Influence of Pathogenic Mutations in alpha-Synuclein on Biophysical and Structural Characteristics of Amyloid Fibrils. *ACS Nano* **2020**, *14* (5), 5213−5222.
(29) Ruggeri, F. S.; Mannini, B.; Schmid, R.; Vendruscolo, M.; Knowles, T. P. J. Single molecule secondary structure determination of proteins through infrared absorption nanospectroscopy. *Nat. Commun.* **2020**, *11* (1), No. 2945.
(30) Ruggeri, F. S.; Vieweg, S.; Cendrowska, U.; Longo, G.; Chiki, A.; Lashuel, H. A.; Dietler, G. Nanoscale studies link amyloid maturity with polyglutamine diseases onset. *Sci. Rep.* **2016**, *6*, No. 31155.
(31) Centrone, A. Infrared imaging and spectroscopy beyond the diffraction limit. *Annu. Rev. Anal. Chem.* **2015**, *8* (1), 101−126.
(32) Park, J. H.; von Maltzahn, G.; Ong, L. L.; Centrone, A.; Hatton, T. A.; Ruoslahti, E.; Bhatia, S. N.; Sailor, M. J. Cooperative nanoparticles for tumor detection and photothermally triggered drug delivery. *Adv. Mater.* **2010**, *22* (8), 880−885.
(33) Wieland, K.; Ramer, G.; Weiss, V. U.; Allmaier, G.; Lendl, B.; Centrone, A. Nanoscale chemical imaging of individual chemotherapeutic cytarabine-loaded liposomal nanocarriers. *Nano Res.* **2019**, *12* (1), 197−203.
(34) Rizevsky, S.; Zhaliazka, M.; Dou, T.; Matveyenka, M.; et al. Characterization of Substrates and Surface-Enhancement in Atomic Force Microscopy Infrared (AFM-IR) Analysis of Amyloid Aggregates. *J. Phys. Chem. C* **2022**, *126*, 4157−4162, DOI: 10.1021/acs.jpcc.1c09643.
(35) Ruggeri, F. S.; Benedetti, F.; Knowles, T. P. J.; Lashuel, H. A.; Sekatskii, S.; Dietler, G. Identification and nanomechanical characterization of the fundamental single-strand protofilaments of amyloid alpha-synuclein fibrils. *Proc. Natl. Acad. Sci. U.S.A.* **2018**, *115* (28), 7230−7235.
(36) Ruggeri, F. S.; Charmet, J.; Kartanas, T.; Peter, Q.; Chia, S.; Habchi, J.; Dobson, C. M.; Vendruscolo, M.; Knowles, T. P. J. Microfluidic deposition for resolving single-molecule protein architecture and heterogeneity. *Nat. Commun.* **2018**, *9* (1), No. 3890.
(37) Ruggeri, F. S.; Longo, G.; Faggiano, S.; Lipiec, E.; Pastore, A.; Dietler, G. Infrared nanospectroscopy characterization of oligomeric and fibrillar aggregates during amyloid formation. *Nat. Commun.* **2015**, *6*, No. 7831.
(38) Zhou, L.; Kurouski, D. Structural Characterization of Individual alpha-Synuclein Oligomers Formed at Different Stages of Protein Aggregation by Atomic Force Microscopy-Infrared Spectroscopy. *Anal. Chem.* **2020**, *92* (10), 6806−6810.
(39) Urano, F.; Bertolotti, A.; Ron, D. IRE1 and efferent signaling from the endoplasmic reticulum. *J. Cell Sci.* **2000**, *113*, 3697−3702.
(40) Calfon, M.; Zeng, H.; Urano, F.; Till, J. H.; Hubbard, S. R.; Harding, H. P.; Clark, S. G.; Ron, D. IRE1 couples endoplasmic reticulum load to secretory capacity by processing the XBP-1 mRNA. *Nature* **2002**, *415* (6867), 92−96.
(41) Shen, X.; Ellis, R. E.; Lee, K.; Liu, C. Y.; Yang, K.; Solomon, A.; Yoshida, H.; Morimoto, R.; Kurnit, D. M.; Mori, K.; Kaufman, R. J. Complementary signaling pathways regulate the unfolded protein response and are required for C. elegans development. *Cell* **2001**, *107* (7), 893−903.
(42) Adams, C. J.; Kopp, M. C.; Larburu, N.; Nowak, P. R.; Ali, M. M. U. Structure and Molecular Mechanism of ER Stress Signaling by the Unfolded Protein Response Signal Activator IRE1. *Front. Mol. Biosci.* **2019**, *6*, No. 11.
(43) Kopp, M. C.; Larburu, N.; Durairaj, V.; Adams, C. J.; Ali, M. M. U. UPR proteins IRE1 and PERK switch BiP from chaperone to ER stress sensor. *Nat. Struct. Mol. Biol.* **2019**, *26* (11), 1053−1062.
(44) Lee, A. H.; Iwakoshi, N. N.; Glimcher, L. H. XBP-1 regulates a subset of endoplasmic reticulum resident chaperone genes in the unfolded protein response. *Mol. Cell. Biol.* **2003**, *23* (21), 7448−7459.
(45) Iwakoshi, N. N.; Lee, A. H.; Glimcher, L. H. The X-box binding protein-1 transcription factor is required for plasma cell differentiation and the unfolded protein response. *Immunol. Rev.* **2003**, *194*, 29−38.

https://doi.org/10.1021/acschemneuro.3c00671
ACS Chem. Neurosci. XXXX, XXX, XXX−XXX

(46) Lee, A. H.; Iwakoshi, N. N.; Anderson, K. C.; Glimcher, L. H. Proteasome inhibitors disrupt the unfolded protein response in myeloma cells. *Proc. Natl. Acad. Sci. U.S.A.* **2003**, *100* (17), 9946−9951.
(47) Harding, H. P.; Zhang, Y.; Ron, D. Protein translation and folding are coupled by an endoplasmic-reticulum-resident kinase. *Nature* **1999**, *397* (6716), 271−274.
(48) Sok, J.; Wang, X. Z.; Batchvarova, N.; Kuroda, M.; Harding, H.; Ron, D. CHOP-Dependent stress-inducible expression of a novel form of carbonic anhydrase VI. *Mol. Cell. Biol.* **1999**, *19* (1), 495−504.
(49) Urano, F.; Wang, X.; Bertolotti, A.; Zhang, Y.; Chung, P.; Harding, H. P.; Ron, D. Coupling of stress in the ER to activation of JNK protein kinases by transmembrane protein kinase IRE1. *Science* **2000**, *287* (5453), 664−666.
(50) Al-Furoukh, N.; Ianni, A.; Nolte, H.; Holper, S.; Kruger, M.; Wanrooij, S.; Braun, T. ClpX stimulates the mitochondrial unfolded protein response (UPRmt) in mammalian cells. *Biochim. Biophys. Acta, Mol. Cell Res.* **2015**, *1853* (10), 2580−2591.
(51) Schreiner, B.; Westerburg, H.; Forne, I.; Imhof, A.; Neupert, W.; Mokranjac, D. Role of the AAA protease Yme1 in folding of proteins in the intermembrane space of mitochondria. *Mol. Biol. Cell* **2012**, *23* (22), 4335−4346.
(52) Broadley, S. A.; Hartl, F. U. Mitochondrial stress signaling: a pathway unfolds. *Trends Cell Biol.* **2008**, *18* (1), 1−4.
(53) Matveyenka, M.; Rizevsky, S.; Kurouski, D. Unsaturation in the Fatty Acids of Phospholipids Drastically Alters the Structure and Toxicity of Insulin Aggregates Grown in Their Presence. *J. Phys. Chem. Lett.* **2022**, *13*, 4563−4569.
(54) Matveyenka, M.; Rizevsky, S.; Kurouski, D. The degree of unsaturation of fatty acids in phosphatidylserine alters the rate of insulin aggregation and the structure and toxicity of amyloid aggregates. *FEBS Lett.* **2022**, *596* (11), 1424−1433.
(55) Matveyenka, M.; Rizevsky, S.; Kurouski, D. Length and Unsaturation of Fatty Acids of Phosphatidic Acid Determines the Aggregation Rate of Insulin and Modifies the Structure and Toxicity of Insulin Aggregates. *ACS Chem. Neurosci.* **2022**, *13* (16), 2483−2489.
(56) Rizevsky, S.; Matveyenka, M.; Kurouski, D. Nanoscale Structural Analysis of a Lipid-Driven Aggregation of Insulin. *J. Phys. Chem. Lett.* **2022**, *13* (10), 2467−2473.
(57) Lu, H.; Wang, X.; Li, M.; Ji, D.; Liang, D.; Liang, C.; Liu, Y.; Zhang, Z.; Cao, Y.; Zou, W. Mitochondrial Unfolded Protein Response and Integrated Stress Response as Promising Therapeutic Targets for Mitochondrial Diseases. *Cells* **2023**, *12* (1), No. 20, DOI: 10.3390/cells12010020.

https://doi.org/10.1021/acschemneuro.3c00671
ACS Chem. Neurosci. XXXX, XXX, XXX−XXX